J Mater Sci: Mater Electron (2017) 28:10877–10884
DOI 10.1007/s10854-017-6866-x

Enhancement of the optical and mechanical properties of chitosan using Fe_2O_3 nanoparticles

Ali Badawi[1] · Emad M. Ahmed[1,2] · Nasser Y. Mostafa[3,4] · F. Abdel-Wahab[1,5] · Sultan E. Alomairy[1]

Received: 6 January 2017 / Accepted: 28 March 2017 / Published online: 3 April 2017

Abstract In this work, the optical and mechanical properties of Fe_2O_3 nanoparticles (NPs)/chitosan nanocomposite films have been investigated. Nanocomposite films of different weight ratios of Fe_2O_3 NPs/chitosan (0, 1, 5, 10, 20 and 30 wt%) were fabricated using casting technique. The optical properties of colloidal Fe_2O_3 NPs and Fe_2O_3 NPs/chitosan nanocomposite films were recorded using UV–visible spectrophotometer. As the ratio of Fe_2O_3 NPs to chitosan increases from 0 to 30%, the energy band gap of Fe_2O_3 NPs/chitosan films decreases from 3.16 to 2.11 eV. This decrease is due to quantum confinement effect. The mechanical properties of the nanocomposite films as a function of sweeping temperature were measured using a dynamic mechanical analyzer. An enhancement in storage modulus, stiffness and glass transition temperature (T_g) has been observed as the ratio of Fe_2O_3 NPs/chitosan increases. T_g of Fe_2O_3 NPs/chitosan nanocomposite film shifts towards higher temperature side with respect to pure chitosan film from 152.1 to 166.3 °C as the ratio of Fe_2O_3 NPs/chitosan increases from 0 to 30 wt%. The increase in T_g is mainly attributed to the decrease in free volumes and vacancies in the nanocomposite films as the weight ratio of Fe_2O_3 NPs/chitosan increases.

✉ Ali Badawi
adaraghmeh@yahoo.com

[1] Department of Physics, Faculty of Science, Taif University, Taif, Saudi Arabia

[2] Department of Physics, National Research Centre, 33 EL Bohouth St. (former EL Tahrir st.), Dokki, Giza 12622, Egypt

[3] Department of Chemistry, Faculty of Science, Taif University, Taif, Saudi Arabia

[4] Department of Chemistry, Faculty of Science, Suez Canal University, Ismailia 41522, Egypt

[5] Department of Physics, Faculty of Science, University of Aswan, Aswan, Egypt

1 Introduction

Currently, polymers nanocomposites films possess attractive considerable research aspects due to the ability of controlling their optical, electrical and mechanical properties [1, 2]. This new class of materials can play an important candidate in many applications, especially in optoelectronic, technological and medical ones [3–5]. Nanocomposites have been investigated for possible applications in photovoltaic cells [6], sensors [7], transport layers and light emitting diodes (LED's) [8]. Chitin and chitosan are biopolymers and consider to be one of the most important natural polymers of the world [9, 10], because of their abundance, biodegradability, absorption and non-toxicity [4, 10]. Chitosan as a biopolymer that derived from chitin can be used for many industrial and medical applications; such as water purification from wastes as dyes and heavy metals, drug delivery carrier, protecting coaters from oxygen sensible products and others [11–13]. Many studies were carried out using chitosan as a host material for many uses [11–13]. Prabaharan [11] used chitosan as nanoparticles (NPs) matrix for drug delivery carriers for cancer therapy. Wan Ngah et al. [12] have utilized chitosan as adsorbing material to get rid of dyes and heavy metals from waste water.

Recently, transition metal oxides as NiO, MnO_2, Fe_3O_4 and Fe_2O_3 were studied to be used as supercapacitors electrodes materials [14, 15]. At ambient conditions, Iron oxide (Fe_2O_3) is stable, low cost, non toxic, easily to prepared and environmentally safe material [16]. Fe_2O_3 has an energy

band gap of 2.1 eV, which makes it as good candidate in absorbing solar visible spectrum [17, 18]. Enhancements of the optical, electrical and mechanical properties of polymers using fillers were the purposes of many researches for different applications [1, 6, 19–21]. In our previous work [1], we enhanced the optical and mechanical properties of PMMA polymer by dopping CdSe quantum dots. Mazov et al. [22] showed that thermal conductivity of multi walled CNTs/polypropylene (PP) is improved about three times higher, as compared with pure PP matrix.

In this study, we have prepared Fe_2O_3 NPs/chitosan nanocomposite films of different weight ratios of (0–30 wt%) using the simple casting technique. The optical properties of colloidal Fe_2O_3 NPs and Fe_2O_3 NPs/chitosan nanocomposite films have been investigated. Also, the effect of Fe_2O_3 NPs ratio on the mechanical properties (the storage modulus (E′), loss modulus (E″), stiffness and loss factor (tan δ)) of the nanocomposite films using the dynamic mechanical analysis (DMA) technque is studied. Moreover, the glass transition temperature (T_g) of the prepared films is also deduced.

2 Experiment

2.1 Synthesis of Fe_2O_3 nanoparticles

Iron oxide (Fe_2O_3) nanoparticles (NPs) were prepared using the method of Mehdizadeh et al. [23] and discussed briefly as follows: 3.0 g of ferric nitrate (Fe $(NO_3)_3{\cdot}9H_2O$) were dissolved in 200 ml of distilled water. 15 g of NaOH were added slowly to the ferric nitrate solution under continuous stirring. After 15 min, the precipitated ferric hydroxide suspension was transferred to 300-ml Teflon-lined stainless steel autoclave. The autoclave was heated to 170 °C under magnetic stirring (180 rpm) for 20 h, and then cooled to the room temperature. The resultant products of Fe_2O_3 NPs were washed with distilled water several times before drying at 100 °C for 24 h.

2.2 Preparation of Fe_2O_3 NPs/chitosan nanocomposite films

Nanocomposite films of Fe_2O_3 NPs/chitosan with different weight ratios of Fe_2O_3 NPs were prepared using a simple solution casting technique as the method discussed in Singh et al. [24]. Briefly, chitosan solution was prepared by dissolving chitosan powder (Sigma-Aldrich) into 100 ml of 0.1 M acetic acid in continuous stirring for 24 h. Nanocomposite films of Fe_2O_3 NPs/chitosan were prepared by adding the desired weight (wt) of Fe_2O_3 NPs powder to the previous chitosan solution and stirring for 4 h on a magnetic stirrer. Then, the produced mixture casted in Petri dishes and left in a ventilated fuming hood until it completely dry and solidify. Nanocomposite films were obtained of x wt% of Fe_2O_3 NPs/chitosan (where x = 1, 5, 10, 20 and 30 wt%) in addition to a pure chitosan film. The dried films were reasonably homogeneous and clear.

2.3 Measurements

The morphology of the synthesized Fe_2O_3 NPs powder was measured using a transmission electron microscope (TEM) (JEOL JEM-2100 operated at 200 kV and equipped with Gatan CCD higher resolution camera). The structural properties of the prepared samples were performed using an automated X- ray diffractometer (Bruker D8-advance diffractometer), at a step of 0.02° from Cu X-ray tube (wavelength kα1 = 1.540598). The absorbance, transmittance and reflectance of the colloidal Fe_2O_3 NPs and Fe_2O_3 NPs/chitosan nanocomposite films were measured using UV–visible–NIR spectrophotometer (JASCO V-670) in the wavelength range from 200 to 900 nm. The mechanical properties (E′, E″, stiffness and tan δ) of the prepared Fe_2O_3 NPs/chitosan nanocomposite films were recorded using a dynamic mechanical analyzer (TA instrument Q800). The samples were adjusted to the tension mode. In this mode, a 1 Hz frequency of oscillation was applied, where the nanocomposite film undergoes a tension between a moveable and fixed clamp using film tension cantilever. A 0.01 N static force is applied in order to prevent buckling. The films were cut to be about 6 mm in width and 25 mm in length. The thickness of the films was about 0.27 mm. A temperature-sweeping mode of a rate of 3 °C/min in the range from 30 to 200 °C was applied. A 15 μm strain amplitude was applied.

3 Results and discussion

3.1 The Morphological and structural properties of Fe_2O_3 NPs/chitosan nanocomposite films

Figure 1 shows the transmission electron microscope (TEM) micrograph of colloidal Fe_2O_3 NPs using JEOL JEM-2100 microscopy. The estimated size of Fe_2O_3 NPs is about 50 ± 2 nm.

Figure 2 shows the X- ray diffraction (XRD) patterns of pure chitosan, pure Fe_2O_3 NPs, 5.0% Fe_2O_3 NPs/chitosan and 30.0% Fe_2O_3 NPs/chitosan nanocomposite films. It is easily seen from Fig. 2(a) that there isn't any distinguishable peaks, which emphasizes the amorphous structure of chitosan polymer. While Fig. 2(b) shows the crystalline structure of Fe_2O_3 NPs. For low ratios of Fe_2O_3 NPs/chitosan (as in Fig. 2(c)), there is no peak evidence due to the homogeneous dispersion of Fe_2O_3 NPs in chitosan matrix

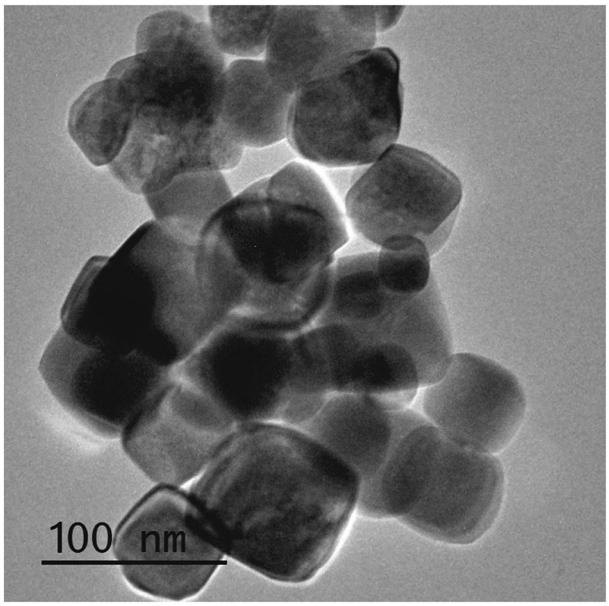

Fig. 1 TEM micrograph of hydrothermally synthesized Fe_2O_3 NPs

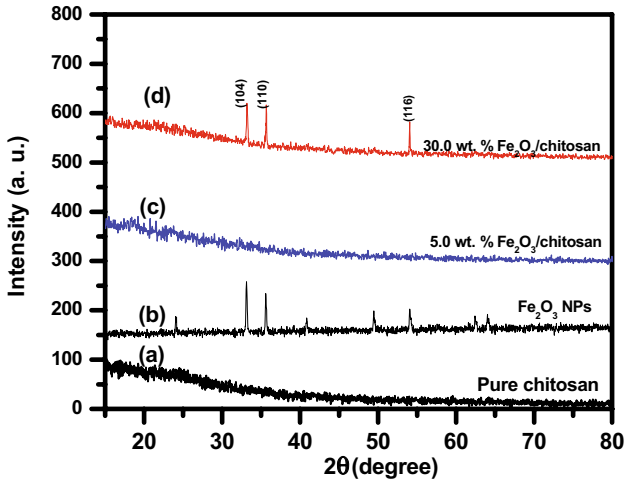

Fig. 2 X-ray diffraction patterns of: (*a*) pure chitosan, (*b*) pure Fe_2O_3 NPs, (*c*) 5.0% of Fe2O3/chitosan and (*d*) 30.0% of Fe_2O_3/chitosan nanocomposite films

and low concentrations of Fe_2O_3 NPs. While three dominant peaks are observed in Fig. 2(d) at $2\theta = 33.14°$, 35.58°, and 54.05°, corresponding to the hexagonal Fe_2O_3 structures (104), (110), and (116) phases respectively (JCPDS No. 33-0664) [25] due to the aggregation of Fe_2O_3 NPs.

3.2 The optical properties of Fe_2O_3 NPs/chitosan nanocomposite films

The absorption (A), transmittance (T) and reflectance (R) spectra of colloidal Fe_2O_3 NPs and different weight ratios (0, 1, 5, 10, 20, 30 wt%) of Fe_2O_3 NPs/chitosan nanocomposite films have been measured using a UV–visible spectrophotometer. These measurements were recorded in the wavelength range from 200 to 900 nm. Figure 3a, b shows the absorption spectra of the colloidal Fe_2O_3 NPs and different weight ratios of Fe_2O_3 NPs/chitosan nanocomposite films respectively. From Fig. 3a, it is clearly seen that the absorption peak of Fe_2O_3 NPs is about 400 nm (corresponding to 3.10 eV) which is blue-shifted with respect to bulk Fe_2O_3 ($E_g = 2.1$ eV [17]) due to the quantum confinement effect, which caused by the decrease in Fe_2O_3 NPs' size. It is obvious that the absorption of Fe_2O_3 NPs/chitosan nanocomposite films increases as the weight ratio of Fe_2O_3 NPs/chitosan increases from 0 to 30% as shown in Fig. 3b. Moreover, the absorption edge is red-shifted to higher wavelength with respect to Fe_2O_3 NPs peak (400 nm), due to the increase of Fe_2O_3 NPs size because of aggregation. Our result is in agreement with others' findings [29, 30]. Al-Hosiny et al. [29] concluded that CdSe quantum dots (QDs) size increases with the

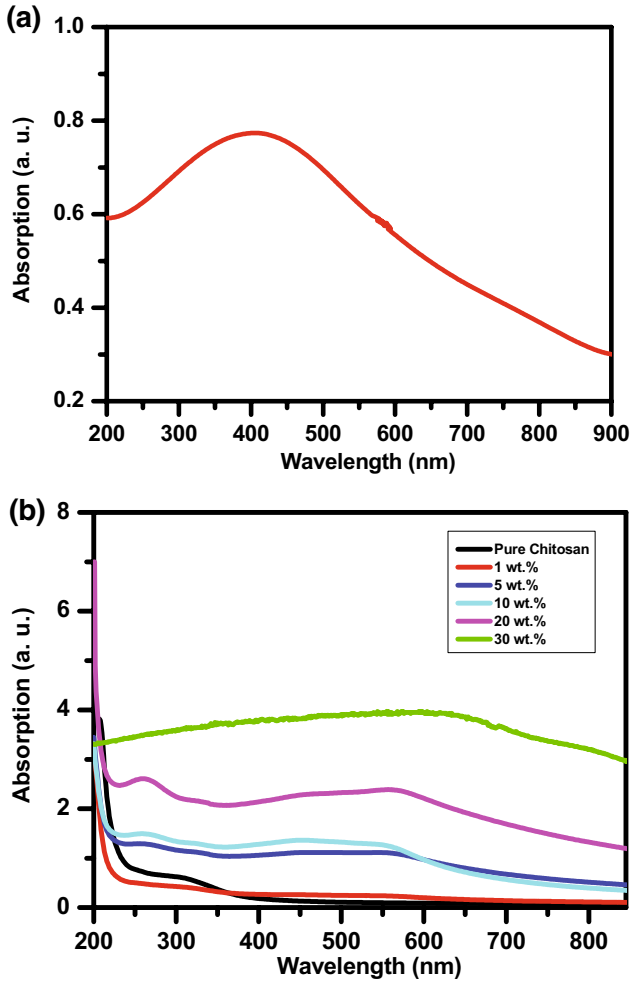

Fig. 3 The absorption spectra of **a** colloidal Fe_2O_3 NPs and **b** different ratios of Fe_2O_3 NPs/chitosan nanocomposite films

increase of its' concentration in PMMA polymer that cause a decrease in CdSe energy band gap. Mthethwa et al. [30] concluded that the absorption of CdS QDs/PMMA nanocomposite films increases as the amount of CdS QDs increases.

Additionally, the energy band gap (E_g) of the colloidal Fe_2O_3 NPs and the prepared Fe_2O_3 NPs/chitosan nanocomposite films were deduced from the transmittance (T) spectra measurements using the following Eq. [32–34]:

$$\alpha h\nu = B(h\nu - E_g)^m \quad (1)$$

where, $\alpha = 2.303\frac{A}{d}$ is the optical absorption coefficient [33], d is film's thickness, h is Planck's constant, B in a constant, m value depends on the type of optical transition. "m" takes values: 1/2, 3/2, 2 or 3 for direct allowed, direct forbidden, indirect allowed and indirect forbidden transitions, respectively. For allowed direct transition, "m" value is chosen to be 1/2 since Fe_2O_3 is a direct band gap semiconductor. E_g values are estimated by extrapolation of the linear region of the curves to $\alpha h\nu = 0$. Figure 4a–f shows $(\alpha h\nu)^2$ of colloidal Fe_2O_3 NPs and different weight ratios (1–30%) of Fe_2O_3 NPs/chitosan nanocomposite films respectively as a function of the incident energy ($h\nu$). The estimated E_g values of colloidal Fe_2O_3 NPs and different weight ratios (1–30%) of Fe_2O_3 NPs/chitosan nanocomposite films are listed in

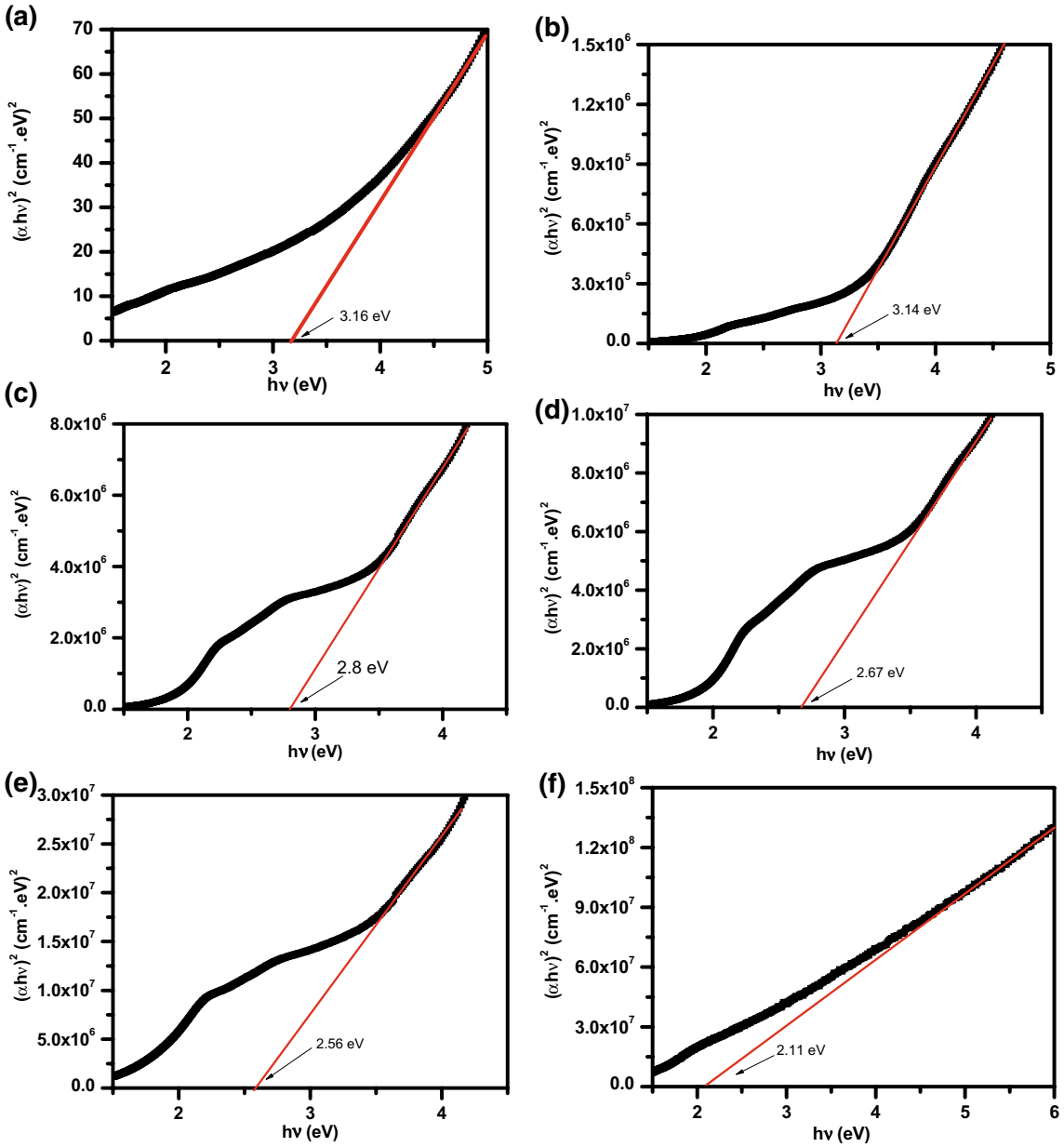

Fig. 4 $(\alpha h\nu)^2$ versus $h\nu$ of **a** colloidal Fe_2O_3 and **b–f** different weight ratios (1–30%) of Fe_2O_3 NPs/chitosan nanocomposite films respectively

Table 1 Energy band gap of colloidal Fe_2O_3 NPs and different weight ratios of Fe_2O_3 NPs /chitosan nanocomposite films

Ratio of Fe_2O_3 NPs/chitosan	Energy band gap (eV)
Colloidal Fe_2O_3 NPs	3.16
1.0 wt%	3.14
5.0 wt%	2.80
10 wt%	2.67
20 wt%	2.56
30 wt%	2.11

Table 1. It is clearly seen that the estimated E_g value of colloidal Fe_2O_3 NPs is 3.16 eV, which is consistent with that obtained from the absorption spectra measurements as shown above. In addition, the E_g value of Fe_2O_3 NPs is blue-shifted with respect to its' bulk value (2.1 eV) due to the quantum confinement effect. The estimated E_g values of Fe_2O_3 NPs/chitosan nanocomposite films are ranged from 3.14 to 2.11 eV as Fe_2O_3 NPs/chitosan weight ratio varies from 1 to 30%. This decrease in E_g value is mainly attributed to the increase in the size of Fe_2O_3 NPs due to aggregation. Our results are in good agreement with other researchers [29, 34]. Abdullah et al. [34] showed that E_g value of CuO NPs doped in PVA polymer decreases as the concentration of CuO NPs increases. They attributed the decrease in E_g value to the modification of the electronic structure of PVA.

Moreover, the effect of Fe_2O_3 NPs/chitosan weight ratio on the refractive index (n) of the prepared Fe_2O_3 NPs /chitosan nanocomposite films is also studied. The n values of the prepared films were estimated from the reflectance (R) spectra measurements and extinction coefficient (K) data in the wavelength range from 200 to 850 nm using Fresnel formula as follows [35, 36]:

$$n = \left(\frac{1+R}{1-R}\right) + \left[\frac{4R}{(1-R)^2} - K^2\right]^{1/2} \quad (2)$$

where, R is the reflectance, K (=αλ/4π) [35] is the extinction coefficient. Figure 5 shows the refractive index (n) of the plain chitosan and different weight ratio (1–30%) of the prepared Fe_2O_3 NPs/chitosan nanocomposite films in the wavelength range from 200 to 850 nm. It is clearly seen that at any wavelength in the range from 200 to 850 nm, the refractive index (n) value increases as the weight ratio of Fe_2O_3 NPs/chitosan increases up to 30%. For example, Fig. 5b shows the linear behavior of the refractive index (n) at wavelength λ equal 600 nm as a function of the weight ratio of Fe_2O_3 NPs/chitosan. This result is mainly attributed to the increase in the reflectance with increasing the weight ratio of Fe_2O_3 NPs/chitosan. Our result is in good agreement with others [3, 34].

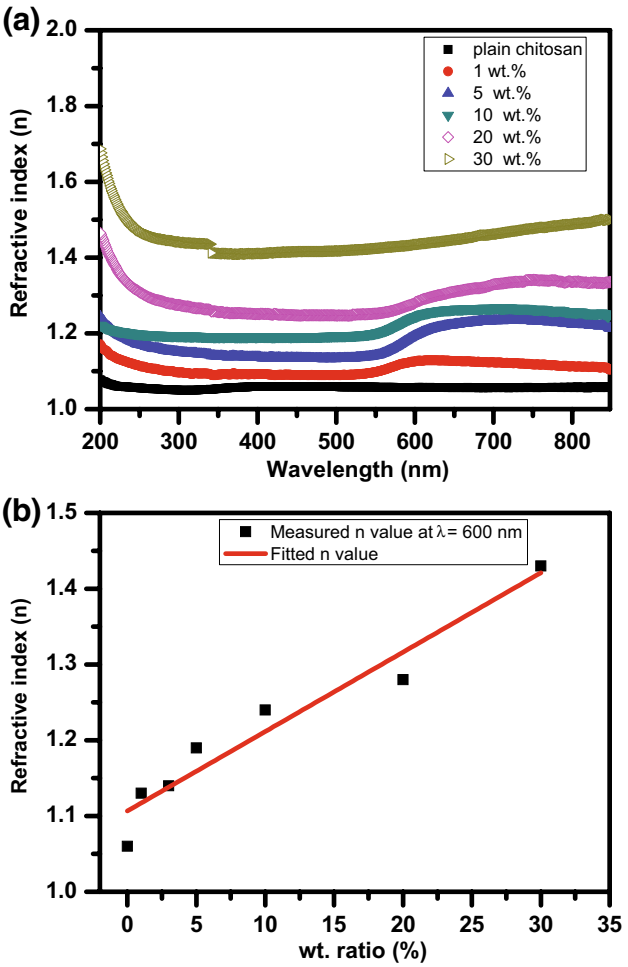

Fig. 5 **a** The refractive index (n) of the plain chitosan and different weight ratio (1–30%) of Fe_2O_3 NPs/chitosan nanocomposite films versus the wavelength, **b** the refractive index (n) at λ = 600 nm as a function of the weight ratio of Fe_2O_3 NPs/chitosan

3.3 Dynamic mechanical analysis of Fe_2O_3 NPs/chitosan nanocomposite films

The analysis of the dynamic mechanical properties (the storage modulus (E′), stiffness, loss modulus (E″) and loss factor (tan δ)) of plain chitosan film and different weight ratios of Fe_2O_3 NPs/chitosan nanocomposite films are studied. A dynamic mechanical analyzer (DMA: TA instrument Q800) is used to measure the mechanical properties of the prepared films by sweeping temperature mode from 40 to 200 °C at an oscillation frequency of 1 Hz. The DMA mechanical response is composed of two parts: the storage modulus (E′) which is related to the stored energy and film's stiffness, while the loss modulus (E″) which is related to the dissipated energy during the cycle of motion.

The general formula of the dynamic (complex) modulus (E*= stress /strain) is given as [37, 38]:

$$E^* = E' + i\,E'' \quad (3)$$

where $E' = \frac{\sigma_0 \cos(\delta)}{\varepsilon_0}$, and $E'' = \frac{\sigma_0 \sin(\delta)}{\varepsilon_0}$. where, σ_0 and ε_0 are the stress and strain amplitudes respectively. δ is the angular shift between the stress and it's corresponding strain.

Figure 6a shows the storage modulus (E′) as a function of temperature of plain chitosan film and different weight ratios (5, 10, 20 and 30 weight %) of Fe_2O_3 NPs /chitosan nanocomposite films at a frequency of 1 Hz under a static force of 0.01 N. It is clearly seen that the storage modulus (E′) is strongly affected with the filler material (Fe_2O_3 NPs) and temperature. Each curve of E′ as a function of sweeping temperature is mainly divided to three regions; the first is the glassy region, where E′ remains stable upto about 100 °C. The second region is called glass transition region, where E′ decreases sharply. The third region is called rubbery region, where the film performs in elastic behavior. At any temperature (T), E′ for all weight ratios of Fe_2O_3 NPs /chitosan nanocomposite films is larger than E′ of plain chitosan film. Also any T degree, E′ increases as the weight ratio of Fe_2O_3 NPs /chitosan increase in the film. The increase in E′ is mostly due to the reduction in the volumes of vacancies in the nanocomposite films [39]. This behavior causes an increase in the stiffness of the nanocomposite films as shown in Fig. 6b. For example, at T = 100 °C, the stiffness of 30 wt % of Fe_2O_3 NPs /chitosan nanocomposite film (13400 N/m) is about twice of that of plain chitosan film (7000 N/m). As the quantity of the vacancies' filler (Fe_2O_3 NPs) increases, the vacancies and free volumes reduce in the nanocomposite films. The decrease in the vacancies makes the nanocomposite films becoming denser and stiffer than that of bare chitosan film. The decrease in the vacancies volumes restricts the motions in the polymers' chains, then limits the energy dissipation, hence increases E′ and stiffness. Our result is in good agreement with others, findings [40–42]. In our previous works [1, 38], we studied the mechanical properties of different weight ratios of SWCNTs and CdSe QDs/PMMA nanocomposite films using a DMA. We concluded that at any T degree, E′ of the nanocomposite films is larger than that of plain PMMA film. Huang et al. [41] concluded that adding 4.76 wt% of modified MWCNTs in PMMA polymer generates enhancement of 184% in E′. They attributed this enhancement to the stiffening effect of MWCNTs.

The loss modulus (E″) of plain chitosan and different weight ratios (5, 10, 20 and 30 wt%) of Fe_2O_3 NPs /chitosan nanocomposite films as a function of temperature is studied. E″ measurements show the role of the dissipated energy in the films. Figure 7 shows E″ obtained from the DMA of the prepared nanocomposite films at an oscillation frequency of 1 Hz. It is obviously seen that E″ depends on the sweeping temperature and the concentration of Fe_2O_3 NPs in the chitosan host matrix. For each film and up to approximately 150 °C, E″ remains within the same level, and then decreases as the temperature increases up to

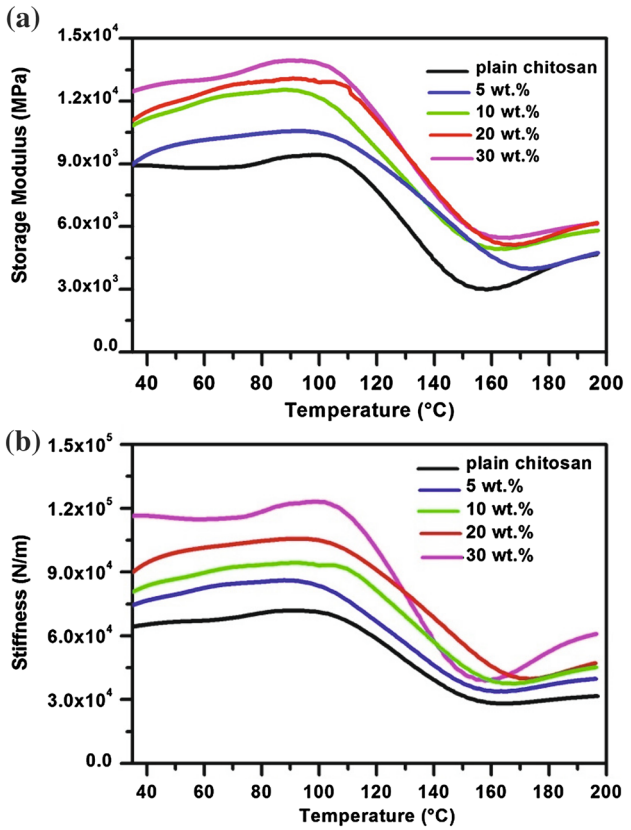

Fig. 6 **a** The storage modulus (E′) and **b** the stiffness as a function of temperature of plain chitosan and different ratios (5, 10, 20 and 30 wt%) of Fe_2O_3 NPs/chitosan nanocomposite films, obtained from a DMA at 1 Hz frequency

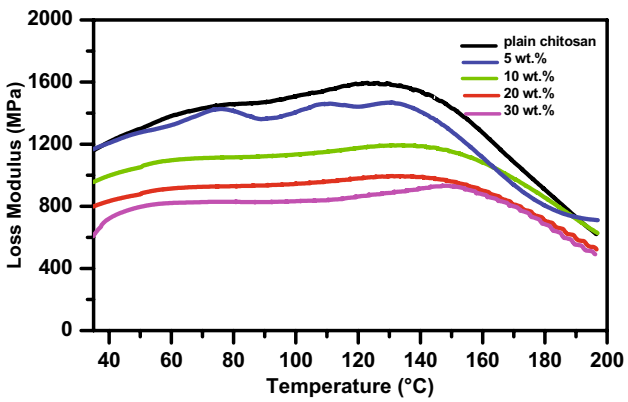

Fig. 7 The loss modulus (E″) versus temperature of plain chitosan and different weight ratios (5, 10, 20 and 30 wt%) of Fe_2O_3 NPs /chitosan nanocomposite films, obtained from a DMA at 1 Hz frequency

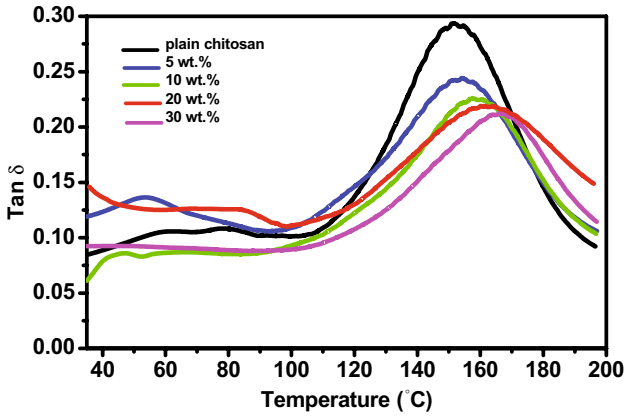

Fig. 8 Tan δ of plain chitosan and different ratios of Fe_2O_3 NPs/chitosan nanocomposite films as a function of temperature, obtained from DMA measurements at 1 Hz frequency

Table 2 Glass transition temperature (T_g) for plain chitosan and different ratios of Fe_2O_3 NPs /chitosan nanocomposite films

Sample	T_g (°C)
Plain chitosan	152.1
5 wt% of Fe_2O_3 NPs/chitosan	154.4
10 wt% of Fe_2O_3 NPs/chitosan	158.2
20 wt% of Fe_2O_3 NPs/chitosan	161.4
30 wt% of Fe_2O_3 NPs/chitosan	166.3

200 °C. More over at each temperature value, as the weight ratio of Fe_2O_3 NPs /chitosan increases from 0 to 30%, E″ value decreases. This result is due to the decrease in the vacancies and free volume as the weight ratio of Fe_2O_3 NPs increases, which leads to the decrease in the dissipated energy and hence decreases in E″.

Additionally, the loss factor (Tan δ) of the prepared films is another important property since the glass transition temperature (T_g) can be deduced. Tan δ is the ratio between the storage modulus and the loss modulus per cycle of the applied force, and given as [38, 43]:

$$tan\ (\delta) = \frac{E''}{E'} \tag{4}$$

The glass transition temperature (T_g) is the temperature at which tan δ reaches its' maximum value [42, 44]. It is the temperature at which a polymers or composite converts from its' glassy state to its' rubbery state. Figure 8 shows tan δ measurements of plain chitosan and different weight ratios (5, 10, 20 and 30 wt%) of Fe_2O_3 NPs/chitosan nanocomposite films as a function of temperature. It is clearly noticeable that the magnitude of tan δ at it's peak is the maximum for plain chitosan film compared with those of different ratios of Fe_2O_3 NPs/chitosan nanocomposite films. In addition, as Fe_2O_3 NPs/chitosan weight ratio increases from 0 to 30%, the magnitude of tan δ decreases from 0.29 to 0.21. The low tan δ value at its' maximum peak is mainly represented the elastic character of the prepared films. While the high value of tan δ shows the viscous character. This novel result improves that the mobility of chitosan molecules is significantly restricted after adding Fe_2O_3 NPs. The results of tan δ is consistent with the data related with E′ and E″. The deduced T_g's values of plain chitosan and different weight ratios of Fe_2O_3 NPs /chitosan nanocomposite films are listed in Table 2. It is clearly seen that T_g value of Fe_2O_3 NPs/chitosan nanocomposite films is shifted towards higher temperature side with respect to plain chitosan film from 152.1 °C to 166.3 °C as the weight ratio increases from 0 to 30%. This increase in T_g value is mainly due to decrease in the vacancies and free volumes as discussed before. Our results are in good agreements with others [38, 42, 45]. In our previous study [38], we concluded that T_g value increases from 91.2 to 99.5 °C as the weight ratio of SWCNTs/PMMA increases from 0 to 2.0%. Also, Dueramae et al. [42] concluded that an enhancement in the glass transition temperature (T_g) of polybenzoxazine (PBA-a) filled with 30 wt% of SiO_2 NPs films with an increase of 16 °C. They attributed enhancement in T_g of the nanocomposite films to the restriction of the motion of PBA-a polymer's chains with the addition of the filler SiO_2 NPs.

Table 2: Glass transition temperature (T_g) for plain chitosan and different ratios of Fe_2O_3 NPs/chitosan nanocomposite films.

4 Conclusions

Different weight ratios (1, 5, 10, 20 and 30 wt%) of Fe_2O_3 nanoparticles (NPs)/chitosan films have been prepared using casting technique. The optical and mechanical properties of the fabricated nanocomposite films are studied. An enhancement in the absorption and refractive index (n) of nanocomposite films are achieved as the weight ratio of Fe_2O_3 NPs/chitosan increases from 0 to 30%. A decrease in the energy band gap (E_g) of the prepared nanocomposite films from 3.16 to 2.11 eV is observed as the weight ratio Fe_2O_3 NPs/chitosan increases up to 30%, due to the quantum confinement effect. The mechanical properties (storage modulus (E′), stiffness, loss modulus (E″) and tan δ) of the nanocomposite films as a function of temperature are measured using a dynamic mechanical analyzer. An enhancement in the storage modulus, stiffness and glass transition temperature (T_g) are achieved for different weight ratios of Fe_2O_3 NPs/chitosan nanocomposite films, compared with those of plain chitosan film. Also, T_g value of Fe_2O_3 NPs/chitosan nanocomposite films shifts towards higher

temperature side with respect to plain chitosan film from 152.1 to 166.3 °C as Fe_2O_3 NPs/chitosan ratio increase from 0 to 30 wt%.

Acknowledgements The authors wish to thank Taif University for the financial support. Members of materials science and engineering research group at Deanship of Scientific Research- Taif University are also thanked for their assistance during this work.

References

1. A. Badawi, J. Mater. Sci. **26**, 3450–3457 (2015)
2. J. Al-Osaimi, N. Al-Hosiny, S. Abdallah, A. Badawi, Iran. Polym. J. **23**, 437–443 (2014)
3. Z.K. Heiba, M.B. Mohamed, N.G. Imam, N.Y. Mostafa, Colloid Polym. Sci. **294**, 357–365 (2016)
4. J. Wang, L. Wang, H. Yu, A. Zain ul, Y. Chen, Q. Chen, W. Zhou, H. Zhang, X. Chen, Int. J. Biol. Macromol. **88**, 333–344 (2016)
5. J. Al-Osaimi, N. Alhosiny, A. Badawi, S. Abdallah, Int. J. Eng Technol IJET-IJENS **13**, 77–79 (2013)
6. A. Badawi, N. Al-Hosiny, S. Abdallah, A. Merazga, H. Talaat, Mater. Sci. Semicond. Process. **26**, 162–168 (2014)
7. R. Smajda, Z. Györi, A. Sápi, M. Veres, A. Oszkó, J. Kis-Csitári, Á. Kukovecz, Z. Kónya, I. Kiricsi. J. Mol. Struct. **834–836**, 471–476 (2007)
8. P.K. Khanna, N. Singh, J. Lumin. **127**, 474–482 (2007)
9. M. Rinaudo, Prog. Polym. Sci. **31**, 603–632 (2006)
10. P.K. Dutta, J. Dutta, V.S. Tripathi, JSIR **63**, 20–31 (2004)
11. M. Prabaharan, Int. J. Biol. Macromol. **72**, 1313–1322 (2015)
12. W.S. Wan Ngah, L.C. Teong, M.A.K.M. Hanafiah, Carbohydr. Polym. **83**, 1446–1456 (2011)
13. F. Cesano, G. Fenoglio, L. Carlos, R. Nisticò, Appl. Surf. Sci. **345**, 175–181 (2015)
14. W. Chen, X. Tao, Y. Li, H. Wang, D. Wei, C. Ban, J. Mater. Sci. **27**, 6816–6822 (2016)
15. P. Lorkit, M. Panapoy, B. Ksapabutr, Energy Proced. **56**, 466–473 (2014)
16. A.A. Yadav, J. Mater. Sci. **27**, 1-8 (2016)
17. J.I. Peña-Flores, A.F. Palomec-Garfias, C. Márquez-Beltrán, E. Sánchez-Mora, E. Gómez-Barojas, F. Pérez-Rodríguez, Nanoscale Res. Lett. **9**, 1–7 (2014)
18. C. Xia, Y. Jia, M. Tao, Q. Zhang, Phys. Lett. A **377**, 1943–1947 (2013)
19. S.I.J. Wilberforce, S.M. Best, R.E. Cameron, J. Mater. Sci. **21**, 3085–3093 (2010)
20. F.O. Rodrigues, R.V. Salvatierra, A.J.G. Zarbin, M.L.M. Rocco, J. Mol. Struct. **1037**, 93–98 (2013)
21. A. Badawi, Chin. Phys. B, **24**, 47205–047205 (2015)
22. I.N. Mazov, I.A. Ilinykh, V.L. Kuznetsov, A.A. Stepashkin, K.S. Ergin, D.S. Muratov, V.V. Tcherdyntsev, D.V. Kuznetsov, J.P. Issi, J. Alloys Compds. **586**, Supplement 1, S440–S442 (2014)
23. R. Mehdizadeh, L.A. Saghatforoush, S. Sanati, Superlattices Microstruct. **52**, 92–98 (2012)
24. J. Singh, M. Srivastava, J. Dutta, P.K. Dutta, Int. J. Biol. Macromol. **48**, 170–176 (2011)
25. J. Hua, J. Gengsheng, Mater. Lett. **63**, 2725–2727 (2009)
26. A.K. Tomar, S. Mahendia, S. Kumar, Adv. Appl. Sci. Res. **2**, 327–333 (2011)
27. E. Lafuente, M.A. Callejas, R. Sainz, A.M. Benito et al., Carbon **46**, 1909–1917 (2008)
28. W.-C. Oh, M.-L. Chen, Bull. Korean Chem. Soc **29**, 159–164 (2008)
29. N.M. Al-Hosiny, S. Abdallah, M.A.A. Moussa, A. Badawi, J. Polym. Res. **20**, 1–8 (2013)
30. T.P. Mthethwa, M.J. Moloto, A.D. Vries, K.P. Matabola, Mater. Res. Bull. **46**, 569–575 (2011)
31. A. Badawi, N. Al-Hosiny, A. Merazga, A. M. Albaradi, S. Abdallah, H. Talaat, Superlattices Microstruct. **100**, 694–702 (2016)
32. A. Badawi, J. Mater. Sci. **27**, 7899–7907 (2016)
33. M.L. Gaur, P.P. Hankare, I.S. Mulla, F.M. Dange, V.M. Bhuse, J. Mater. Sci. **27**, 7603–7608 (2016)
34. O.G. Abdullah, S.B. Aziz, K.M. Omer, Y.M. Salih, J. Mater. Sci. **26**, 5303–5309 (2015)
35. A A. Atta, M.M. El-Nahass, K.M. Elsabawy, M.M. Abd El-Raheem, A.M. Hassanien, A. Al Huthali, A. Badawi, A. Merazga, Pramana **87**, 72 (2016)
36. M.M. Abd El-Raheem, S.A. Amin, M.A. Alharbi, A.M. Badawi, J. Opt. Technol. **83**, 375–384 (2016)
37. H. Essabir, A. Elkhaoulani, K. Benmoussa, R. Bouhfid, F.Z. Arrakhiz, A. Qaiss, Mater. Des. **51**, 780–788 (2013).
38. A. Badawi N. Al Hosiny, Chin. Phys. B **24**, 105101 (2015)
39. M. Dixit, S. Gupta, V. Mathur, K.S. Rathore, K. Sharma, N.S. Saxena, Chalcogen Lett. **6**, 131–136 (2009)
40. N.G. Sahooa, S. Ranab, J.W. Chob, L. Li, S.H. Chana, Prog. Polym. Sci. **35**, 837–867 (2010)
41. Y.-L. Huang, C.-C.M. Ma, S.-M. Yuen, C.-Y. Chuang, H.-C. Kuan, C.-L. Chiang, S.-Y. Wu, Mater. Chem. Phys. **129**, 1214–1220 (2011)
42. I. Dueramae, C. Jubsilp, T. Takeichi, S. Rimdusit, Compos Part B, **56**, 197–206 (2014)
43. K. Sewda, S.N. Maiti, Polym. Bull. **70**, 2657–2674 (2013)
44. R. Faria, J.C. Duncan, R.G. Brereton, Polym. Test. **26**, 402–412 (2007)
45. A.L. Martínez-Hernández, C. Velasco-Santos, V.M. Castaño, Curr. Nanosci. **6**, 12–39 (2010)